JOURNAL OF GUIDANCE, CONTROL, AND DYNAMICS
Vol. 30, No. 3, May–June 2007

Repeat-Groundtrack Orbit Acquisition and Maintenance for Earth-Observation Satellites

M. Aorpimai*
Mahanakorn University of Technology, Bangkok 10530, Thailand
and
P. L. Palmer†
University of Surrey, Guildford, GU2 7XH England, United Kingdom

DOI: 10.2514/1.23413

In this paper, the condition for repeat-groundtrack orbits is investigated. The analysis is based upon a set of orbital elements called epicycle elements. As well as avoiding circular orbit singularity, this analysis allows higher geopotential harmonics to be included up to an arbitrary number until a satisfactory accuracy has been achieved. It allows a repeat-groundtrack condition to be precisely evaluated with a simple and instructive mathematical description. In the second part of the paper, an orbit control strategy is proposed. Its aim is to autonomously maneuver a satellite from any initial condition toward a repeat-groundtrack condition. The emphasis is on a multiple-burn strategy with small velocity increments, which is preferable for small satellites for which the onboard and ground station facilities are limited. An autonomous orbit maintenance strategy to keep the satellite at a repeat-groundtrack condition despite perturbations from atmospheric drag is also presented. Finally, the experimental results obtained from a 300-kg satellite are shown. Both the orbit acquisition and maintenance demonstrations confirm the performance of the proposed strategies.

Introduction

REPEAT-GROUNDTRACK orbit is useful for Earth-observation and Earth-science missions, because it allows the satellite to reobserve any particular spot, either on or above the ground, within the same predefined period of time. There are a number of existing missions that are operating in repeat-groundtrack orbits, such as LANDSAT, SPOT, ENVISAT, RADARSAT,and JASON-1 (the successor of TOPEX/Poseidon). Some Earth-like missions, such as Martian [1], also take advantage of this type of orbit.

The evaluation of conditions for a repeat-groundtrack orbit under perturbations, especially from the nonspherical Earth, is not so straightforward. Many previous works, such as that mentioned in [2], treated the problem with only the second term of the zonal geopotential harmonics taken into account. The accuracy of the solution, however, has proven to be insufficient for some missions. The retired TOPEX/Poseidon mission, for instance, requires a repeat-groundtrack pattern, which enables the spacecraft to fly over two verification sites within an accuracy of ± 1 km around the reference equator crossings [3]. With such a stringent requirement, higher terms and degrees of geopotential harmonics have to be included in the orbital analysis and control. Such analysis has been done elaborately by Vincent [4], and a further investigation on orbital evolution caused by tesseral harmonics has been presented by Ely and Howell [5]. The results from the latter work are particularly useful for orbits with significant eccentricities. From a more abstract perspective, repeat-groundtrack orbits arise from bifurcations [6].

In this paper, an analytical solution for repeat-groundtrack condition of Earth satellites in near-circular orbits is presented. The analysis is based upon a set of orbital elements that, as well as avoiding circular orbit singularity, allow higher geopotential harmonics to be included up to an arbitrary number until a satisfactory accuracy has been achieved. It allows the repeat-groundtrack condition to be precisely evaluated with a relatively simple and instructive mathematical description. The analysis then leads to the efficient design of orbit acquisition and maintenance algorithms.

The orbit control strategies presented in this paper are intended for an autonomous orbit control (AOC) system, because it will become more common for future missions. Principally, when a spacecraft can navigate itself in real time and react by firing its onboard thruster spontaneously to disturbances, a high accuracy of orbit control performance can be expected. AOC also requires minimal resources both onboard and at the ground station, compared with a typical ground-based orbit control strategy. Recently, AOC has been demonstrated in a number of missions. The navigation and control system in the Demeter satellite, for example, gave some promising results during the experiment to control the longitudes of the satellite groundtracks at the equator [7]. In this paper, an experiment in orbit maintenance to keep the satellite in a tight window around a repeat-groundtrack condition is demonstrated. The satellite UoSAT-12 uses only an onboard global positioning system (GPS) receiver and a chemical low-thrust propulsion system for an AOC system [8].

Presented as Paper 111 at the 14th Space Flight Mechanics Meeting, Maui, HA, 2 August–2 December 2004; received 24 February 2006; revision received 4 November 2006; accepted for publication 5 November 2006.

*Lecturer, Small Satellite Research Centre.
†Senior Lecturer, Surrey Space Centre.

Orbital Dynamics

Epicycle Description

The description of the near-circular motion of a satellite under an axisymmetric potential can be summarized through a linearized set of equations called epicycle equations. Like other nonsingular elements, the epicycle elements are introduced in such a way that terms that have a small divisor of eccentricity are removed.

The idea is based upon using two polar elements (see Fig. 1): radius r and azimuthal angle λ (argument of latitude), and two orbital elements: inclination I and right ascension of ascending node Ω, which completes four elements to describe the location of a satellite S at any time. The evolution of these quantities in time is given by [9]

$$r = a(1+\rho) - A\cos(\alpha - \alpha_P) + a\chi\sin[(1+\kappa)\alpha] + \Delta_r \quad (1a)$$

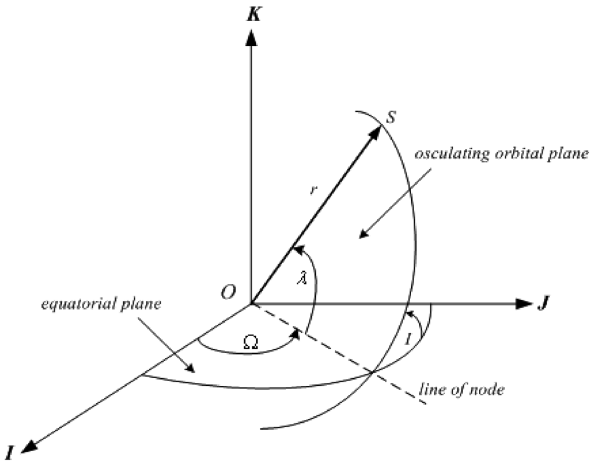

Fig. 1 Coordinate system.

$$\lambda = (1+\kappa)\alpha + \frac{2A}{a}[\sin(\alpha-\alpha_P) + \sin\alpha_P] - 2\chi\{1 - \cos[(1+\kappa)\alpha]\} + \Delta_\lambda \tag{1b}$$

$$I = I_0 + \Delta_I \tag{1c}$$

$$\Omega = \Omega_0 + \vartheta\alpha + \Delta_\Omega \tag{1d}$$

where $\alpha \cong nt$ and n is the mean motion. Time t is measured from an initial equator crossing. In these equations, a is a mean semimajor axis defined through the conserved orbital energy ε when only zonal harmonics are included:

$$a = -\frac{\mu}{2\varepsilon} \tag{2}$$

and μ is the gravitational parameter of the central body that is related to n through Kepler's law: $a^3n^2 = \mu$. I_0 and Ω_0 are the osculating inclination and ascending node at $t = 0$. A and α_P are two integration constants appearing in the derivation of Eq. (1). A is referred to as the epicycle amplitude.

The constant offset in orbital radius caused by even zonal harmonics is described by ρ. The secular change in the ascending node is described by $\vartheta\alpha$, which causes a linear variation of Ω with time. The secular drift in argument of latitude is described by κ. The long-periodic variations are described by χ, and the short-periodic variations are expressed as a Fourier series through the terms Δ_x for each of the four elements. When the epicycle phase α changes by 2π, then the argument of latitude changes secularly by an amount $2\pi + 2\kappa\pi$. The argument of latitude can then be considered to vary with time as $\lambda \sim n_N t$, where

$$n_N = (1+\kappa)n \tag{3}$$

and $2\pi/n_N$ is the nodal period.

The closed-form solutions for the perturbation terms for an axisymmetric Earth when only the first order in zonal geopotential harmonics are taken into account are [9]

$$\rho = \sum_{m=1}\rho_{2m} = \sum_{m=1}(2m-1)J_{2m}\left(\frac{R_e}{a}\right)^{2m} L^0_{2m} \tag{4a}$$

$$\vartheta = \sum_{m=1}\vartheta_{2m} = -\sum_{m=1}2J_{2m}\left(\frac{R_e}{a}\right)^{2m}\frac{\cot I_0}{\sin I_0}\sum_{l=1}^{m} 2lL^{2l}_{2m} \tag{4b}$$

$$\kappa = \sum_{m=1}\kappa_{2m} = -\sum_{m=1}(4m-1)J_{2m}\left(\frac{R_e}{a}\right)^{2m} L^0_{2m} - \vartheta_{2m}\cot I_0 \tag{4c}$$

$$\chi = \sum_{m=1}\chi_{2m+1} = -\sum_{m=1}\frac{2mJ_{2m+1}}{\kappa}\left(\frac{R_e}{a}\right)^{2m+1} L^1_{2m+1} \tag{5}$$

where R_e is the Earth's mean equatorial radius; $m = 1, 2, 3, \ldots$, $l = 1, 2, 3, \ldots$, and J_n are the nth degree of the Earth's zonal gravitational harmonic coefficients; and the coefficients L^j_i are given by

$$L^j_i = \frac{(i-j)!}{(i+j)!}P^j_i(0)P^j_i(\cos I_0) \tag{6}$$

and P^j_i are the associated Legendre polynomials.

Note that in the absence of perturbing terms, the epicycle equations are reduced to

$$r = a - A\cos(\alpha - \alpha_P) \tag{7a}$$

$$\lambda = \alpha + \frac{2A}{a}[\sin(\alpha-\alpha_P) + \sin\alpha_P] \tag{7b}$$

$$I = I_0 \tag{7c}$$

$$\Omega = \Omega_0 \tag{7d}$$

In the two-body case, I and Ω are fixed, and the eccentricity and argument of perigee are also constants related directly to the parameters A and α_P, respectively.

Update Epicycle Parameters

In this section, the effect of an arbitrary in-plane impulsive ΔV on the epicycle parameters shall be derived. By differentiating Eqs. (1a) and (1b), with the short-periodic terms excluded and high-order terms in J_n ignored, the radius and azimuthal velocities can be obtained as

$$V_r = n[A\sin(\alpha-\alpha_P) + a\chi(1+\kappa)\cos\beta] \tag{8a}$$

$$V_\lambda = (1+\kappa)n\{a(1+\rho) + A[1+2(\rho-\kappa)]\cos(\alpha-\alpha_P) - (1+2\rho)a\chi\sin\beta\} \tag{8b}$$

where $V_r = \dot{r}$, $V_\lambda = r\dot{\lambda}$, and $\beta = (1+\kappa)\alpha$. At the instant of firing, the velocity components will change instantaneously, whereas the position remains the same. So after firing, we obtain

$$\hat{r} = r \tag{9a}$$

$$\hat{\lambda} = \lambda \tag{9b}$$

$$\hat{V}_r = V_r + \Delta V_r \tag{9c}$$

$$\hat{V}_\lambda = V_\lambda + \Delta V_\lambda \tag{9d}$$

where ΔV_r and ΔV_λ are the ΔV components along the radius and azimuthal directions, respectively. The hat over a variable refers to its value after firing. The change in a can be solved from the change in orbital energy $\Delta\varepsilon$:

$$\Delta a = \frac{2\Delta\varepsilon}{an^2} = \frac{2}{an^2}(V_r\cdot\Delta V_r + V_\lambda\cdot\Delta V_\lambda) \tag{10}$$

which, to first order in J_n, results in

$$\hat{a} = a + \frac{2\Delta V_\lambda}{n} \tag{11}$$

By knowing $\hat{a}$ and using the same approximation, the velocity Eqs. (8) and (9) can be rearranged to give

$$\hat{A}\cos(\alpha - \hat{\alpha}_P) = A\cos(\alpha - \alpha_P) + \frac{2\Delta V_\lambda}{n} \tag{12a}$$

$$\hat{A}\sin(\alpha - \hat{\alpha}_P) = A\sin(\alpha - \alpha_P) + \frac{\Delta V_r}{n} \tag{12b}$$

where $\hat{A}$ and $\hat{\alpha}_P$ are the post-firing variables of the epicycle parameters A and α_P, respectively. These equations can be further rearranged as

$$\Delta\xi\cos\alpha + \Delta\eta\sin\alpha = \frac{2\Delta V_\lambda}{n} \tag{13a}$$

$$\Delta\xi\sin\alpha - \Delta\eta\cos\alpha = \frac{\Delta V_r}{n} \tag{13b}$$

where $\Delta\xi = \hat{A}\cos\hat{\alpha}_P - A\cos\alpha_P$ and $\Delta\eta = \hat{A}\sin\hat{\alpha}_P - A\sin\alpha_P$.

Evaluation of Repeat-Groundtrack Condition

A repeat-groundtrack orbit is obtained when there is a commensurability between the satellite's nodal frequency and the Earth's rotation rate (i.e., the time for an integer number of orbits of the satellite is equal to the total time for an integer number of rotations of the Earth).

The separation between two consecutive equator crossings L_S is a function of the Earth's rotation rate ω_e and the drift in ascending node $\dot{\Omega}$, as

$$L_S = P_N(\omega_e - \dot{\Omega}) \tag{14}$$

where P_N is the nodal period of the orbit, which is the period between successive equator crossings of the satellite. The condition for the groundtrack to repeat every k orbits in d days can be formulated as

$$kL_S = 2\pi d \tag{15}$$

Substituting L_S from Eq. (14) and rearranging the equation yields

$$\frac{(\omega_e - \dot{\Omega})}{n_N} = \frac{d}{k} \tag{16}$$

where $n_N = 2\pi/P_N$ is the nodal frequency. Note that d is not the sidereal day, but is the number of revolutions that the Earth completes in its rotating cycle as viewed from the precessing orbital plane.

From Eq. (1d), with the short-periodic variations omitted, the drift rate in the ascending node is

$$\dot{\Omega} = \vartheta n \tag{17}$$

The nodal frequency can be obtained from Eq. (3), and the repeat-groundtrack condition can be formulated in terms of the epicycle parameters as

$$\frac{[(\omega_e/n) - \vartheta]}{(1+\kappa)} = \frac{d}{k} \tag{18}$$

Equation (18) allows higher-order terms, as well as a higher degree of zonal harmonics, to be included in evaluating the repeat-groundtrack condition to any desired level of accuracy. In many practical applications, however, it is sufficient to consider only the first few terms of perturbations, which simplifies the evaluation. For example, when the first order in J_2 and J_4, as well as the second order in J_2 (which is of 10^{-6} order), are taken into account in the calculation of ϑ and κ, the repeat-groundtrack condition can be explicitly formulated as

$$\frac{\frac{\omega_e}{J_2}\sqrt{\frac{a^3}{\mu}}\left(\frac{a}{R_e}\right)^2 + \frac{3}{2}\cos I_0 - \frac{15}{16}\frac{J_4}{J_2}\left(\frac{R_e}{a}\right)^2\cos I_0(4 - 7\sin^2 I_0) + \frac{3}{8}\frac{(J_2)^2}{J_2}\left(\frac{R_e}{a}\right)^2\cos I_0(11 - 20\sin^2 I_0)}{1 + (3 - \frac{15}{4}\sin^2 I_0) - \frac{15}{16}\frac{J_4}{J_2}\left(\frac{R_e}{a}\right)^2\left(\frac{34}{5} - 25\sin^2 I_0 + \frac{77}{4}\sin^4 I_0\right) + \frac{3}{16}\frac{(J_2)^2}{J_2}\left(\frac{R_e}{a}\right)^2(14 + 17\sin^2 I_0 - 35\sin^4 I_0)} = \frac{d}{k} \tag{19}$$

With a defined repeat-groundtrack pattern and the operational inclination given, the corresponding mean semimajor axis a can be solved by using any standard numerical method.

Repeat-Groundtrack Orbit Acquisition

Once a repeat-groundtrack condition has been selected and the repeat-groundtrack orbital radius has been solved, a set of equator-crossing longitudes can be assigned as a reference grid around the equator. The grid can also be shifted in phase so that the satellite's groundtrack passes over particular targets, such as verification sites, ground control stations, and observation spots. The groundtrack for which the equator-crossing points have been tied to a particular reference grid will be referred to as the reference track.

The groundtrack pattern of a satellite in an orbit that is not a repeat groundtrack will appear to naturally drift relative to the reference track. The mean groundtrack displacement per nodal period ΔL_S of a satellite in a vicinity orbit around the repeat-groundtrack orbit can be approximated as

$$\Delta L_S = \frac{\partial L_S}{\partial a}\Delta a + \frac{\partial L_S}{\partial i}\Delta i \tag{20}$$

where Δa and Δi, respectively, are the deviations in orbital radius and inclination from the repeat-groundtrack orbit.

The effect from the third-body perturbation is small in low-Earth-orbit (LEO) environments (about an order of 10^{-8}) and not included in our analysis. Consequently, the variation in equator-crossing separation due to the change in inclination is assumed to be negligible. From Eqs. (14) and (20), to first order approximation, we obtain

$$\Delta L_S = \frac{\partial(P_N[\omega_e - \dot{\Omega}])}{\partial a}\Delta a = \frac{3}{2}P_{N_0}(\omega_e - \dot{\Omega}_0)\frac{\Delta a}{a_0} \tag{21}$$

where a_0 and P_{N_0} are the mean semimajor axis and the corresponding nodal period at the repeat-groundtrack condition, respectively. The average groundtrack drift rate $\Delta\dot{L}_S$ is the groundtrack displacement

per period, divided by the nodal period:

$$\Delta\dot{L}_S = \frac{3}{2}\frac{P_{N_0}}{P_N}(\omega_e - \dot{\Omega}_0)\frac{\Delta a}{a_0} \tag{22}$$

The effect from atmospheric drag causes an eastward drift of the groundtrack due to the reduced orbital period. The linearized groundtrack acceleration $\Delta\ddot{L}_S$ due to the decay rate $\dot{a}$ is

$$\Delta\ddot{L}_S = \frac{3}{2}(\omega_e - \dot{\Omega}_0)\frac{\dot{a}}{a_0} \tag{23}$$

By using a simple decay rate estimation model, a series of small burns can be applied to bring a satellite from any initial conditions toward a desired repeat-groundtrack condition. The desired groundtrack displacement during each period of firing step can be obtained by solving Eq. (23) and setting an appropriate initial Δa. The last burn should be applied to reduce the drift rate and bring the satellite smoothly into the orbit maintenance phase. The multiple-burns orbit acquisition strategy can be summarized as

$$\Delta L_{S_0} = \Delta L_{S_1}(\Delta a_1, T_1) + \Delta L_{S_2}(\Delta a_2, T_2) + \Delta L_{S_3}(\Delta a_3, T_3) + \ldots + \Delta L_{S_n}(\Delta a_n, T_n) \tag{24}$$

where ΔL_{S_0} is the initial groundtrack displacement, T_i is the drift period for each step, Δa_i is the initial displacement in a from the repeat-groundtrack value at step i, and ΔL_{S_i} is the groundtrack drift gained during each firing step.

Note that this strategy provides some advantages over a small number of large burns. First, the thruster can be recalibrated to give a more accurate thrust by analyzing the result from previous burns. Second, the groundtrack can be brought to the reference very smoothly, and the orbit maintenance phase can be enabled immediately after the acquisition without any discontinuity between these operational phases.

Orbit Maintenance

For a satellite in LEO, atmospheric drag is a major source of disturbance to the repeat-groundtrack condition. Sectoral and tesseral geopotential harmonics will not cause any secular effect, but will generate periodic variations in the orbital elements. In this section, a strategy to handle the secular drift due to atmospheric drag is described.

From Eq. (23), by assuming a constant decay rate D, the groundtrack drift rate and the groundtrack displacement can be solved as

$$\Delta\dot{L}_S = \frac{3}{2}(\omega_e - \dot{\Omega}_0)\frac{D}{a_0}t + \Delta\dot{L}_{S_0} \tag{25}$$

and

$$\Delta L_S = \frac{3}{4}(\omega_e - \dot{\Omega}_0)\frac{D}{a_0}t^2 + \Delta\dot{L}_{S_0}t + \Delta L_{S_0} \tag{26}$$

where $\Delta\dot{L}_{S_0}$ and ΔL_{S_0} are the initial drift rate and the initial displacement in groundtrack, respectively.

A strategy to keep the satellite at a repeat-groundtrack condition is shown using a phase plane in Fig. 2. The control loop starts from an initial condition in which the satellite groundtrack displacement is σ deg east with respect to the reference track. By putting the satellite at an altitude higher than the repeat-groundtrack radius, the satellite groundtrack will appear to drift westward, because its orbital period is longer than the reference orbit. The atmospheric drag tends to reduce the orbital period and cause the groundtrack drift rate to decrease as time goes by. The drift will cease when the orbital radius is equal to the reference value and starts to drift in the opposite direction when the orbit is lower than the repeat-groundtrack orbit. An impulsive firing shall be executed to restore the control loop when the groundtrack displacement comes back to its initial value.

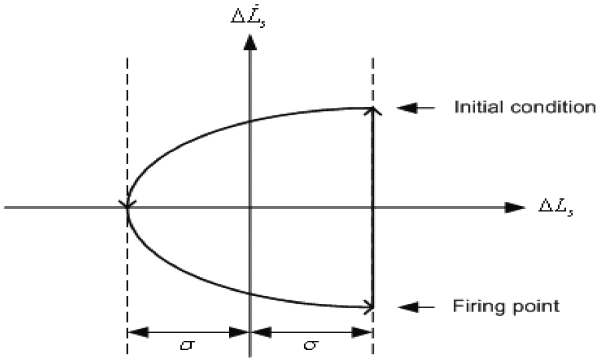

Fig. 2 Phase plane of the groundtrack within a control cycle.

For the orbit maintenance of a small satellite, the small-burn strategy with a short control-cycle period is preferable. In fact, the upper and lower parts of the phase plane diagram shown in Fig. 2 will become more asymmetric as the period of a control cycle becomes longer, because of the variation of the atmospheric density with height. This means that a bigger ΔV is required to restore the control loop.

With real-time estimates of mean semimajor axis and decay rate onboard the satellite, a closed-loop controller can be designed to cope with the variations in atmospheric drag and maintain the control profile, as described earlier. The impulsive control action is proportional to the deviation in the semimajor axis from the repeat-groundtrack value and the orbital decay rate. The controller gains can be determined by solving Eqs. (22) and (25) and using Eq. (11):

$$\Delta V_\lambda = \frac{n_0}{2}\left(\Delta a + \frac{T_c}{2}\dot{a}\right) \tag{27}$$

where T_c is the control-cycle period.

It is important to note that, to the level of our approximation, the change in semimajor axis of a near-circular orbit due to a small impulsive ΔV firing does not depend on the orbital phase of firing. Therefore, we have freedom to choose the firing phase in such a way that all burns used for the repeat-groundtrack orbit maintenance can also change the shape of the orbit. Each burn can be used to optimally move e and ω toward a frozen condition by firing at the appropriate orbital phase [10].

Results

Repeat-Groundtrack Acquisition of UoSAT-12

The orbit acquisition and maintenance strategies described earlier have been successfully demonstrated onboard UoSAT-12, a 300-kg minisatellite [8]. The spacecraft was launched into an inclined 64.57-deg orbit with an altitude of approximately 650 km. The spacecraft acceleration when using two cold-gas thrusters is around 1 mm/s^2; thus, if we assume that a burn length of 5 min is the longest that can be approximated as impulsive, taking as it does roughly 18 deg of an orbit, the largest near-impulsive burn achievable by the satellite is only around 0.3 m/s.

A repeat-groundtrack condition is selected so that the satellite passes directly over the ground station at Surrey Space Centre (SSC) twice every week. The corresponding condition is 7 days for 102 orbital revolutions. The zonal harmonics up to J_4 as well as J_2^2 are included in the evaluation of the repeat-groundtrack condition. By solving Eq. (19), we obtained a repeat-groundtrack radius of $a_0 = 7027.927$ km. To enable two high passes over the ground station at SSC, it requires one of the descending node crossings of the orbit to pass over the equator at 31.950 deg east.

The initial orbital radius of UoSAT-12 was about 430 m above the repeat-groundtrack orbit, and the equator crossing was 0.23 deg east of the target value. From Eq. (26), it would take about seven days for the groundtrack to reach the reference track, based on an estimated decay rate due to drag of 7.2 m/day. The required ΔV was calculated from Eq. (11) to change the estimated semimajor axis at the firing instant to the reference radius, and a 16 cm/s ΔV was

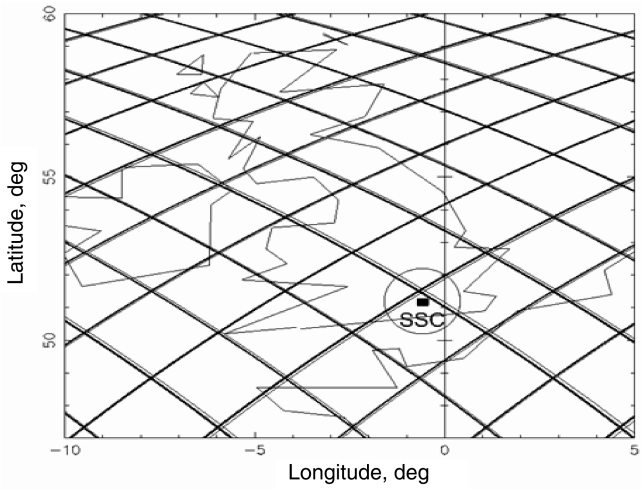

Fig. 3 Satellite groundtrack over SSC before and after the orbit acquisition.

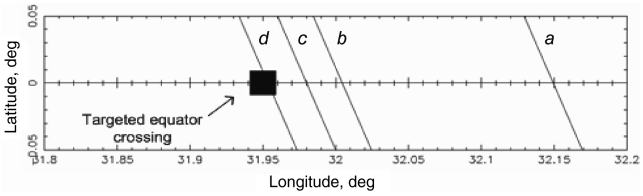

Fig. 4 Satellite groundtrack at the equator crossing before and after the orbit acquisition.

autonomously commanded and executed in the antivelocity direction.

The first set of epicycle parameters was determined after this firing by using a batch filter [11] that retrieved GPS data every 10 s for 24 h. By propagating the satellite orbit forward using this set of parameters, we found that the satellite groundtrack repeats with two high-elevation passes over SSC (shown by thick lines in Fig. 3). The pattern during the approach to the repeat-groundtrack orbit is shown in the lighter lines. Viewed on a magnified scale, however, the groundtrack still has a small westward drift, with a drift rate of about 0.026 deg per week, as shown in Fig. 4, in which the target descending equator crossing is marked by the black square at 31.950 deg east. Before firing, the groundtrack (marked by *a*) crosses at 32.15 deg and is drifting westward. After firing, the drift rate is reduced and the groundtrack (marked by *b*–*d*) slowly approaches the target. This small drift is intentional, because it allows the orbit operation to be switched to the maintenance phase smoothly.

Orbit Maintenance

The orbital maintenance experiment could not start immediately after the orbit acquisition, due to other experiments being performed on the satellite. The semimajor axis starts from approximately 30 m above the repeat-groundtrack condition from the initial epoch. The GPS receiver retrieves navigation data every 10 s. The epicycle orbital elements are determined via the Kalman filtering technique [12]. The orbit controller uses the determined epicycle elements every 24 h to compute the firing commands. A command comprises the ΔV magnitude and direction and the optimal time for firing to move the satellite orbit toward the frozen condition of $e = 0.0016$ and $\omega = -90$ deg [10]. The commands are returned to the attitude control system to rotate the satellite according to the ΔV direction command and to the propulsion system to execute the burn.

Figure 5 shows the semimajor axis history from the starting epoch until the end of the experiment 27 days later. The satellite could regulate the mean altitude at the reference value without any support from the ground, and most of the time, the semimajor axis remains within 5 m of the reference value, and the mean error is 2.6 m. All ΔV commands are in the positive along-track direction, which is the most

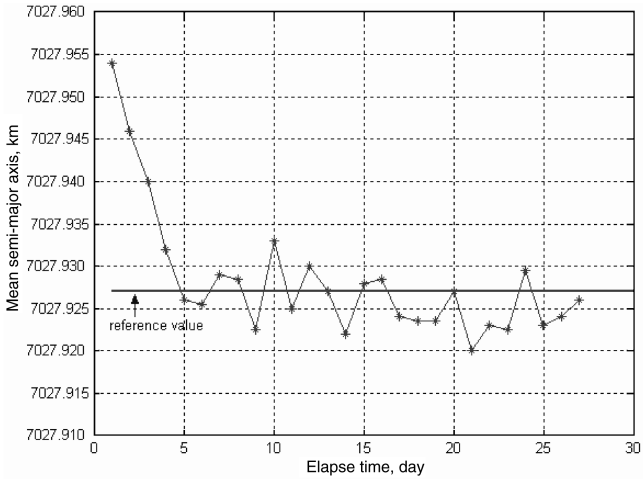

Fig. 5 Mean semimajor axis history during the orbit maintenance experiment.

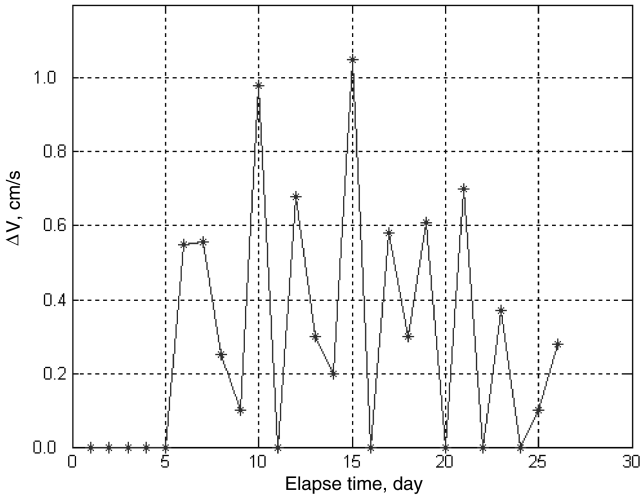

Fig. 6 ΔV history during the orbit maintenance experiment.

effective use of the fuel. The ΔV magnitude history is shown in Fig. 6. The mean ΔV during steady state is 3.6 mm/s per day. The displacement of the groundtrack at the equator crossing during four repeating cycles is kept within 5 km, with a mean value of 2.72 km, which is within the accuracy level expected from our approximation during the orbital analysis and control strategy design.

Conclusions

The analysis of a repeat-groundtrack condition through epicycle elements gives an accurate and instructive solution. Some submeter accuracy can be achieved for a satellite in a low-Earth-orbit environment in which the third-body perturbation is relatively small.

The proposed orbit acquisition and maintenance algorithms are simple and readily implemented. As demonstrated, an autonomous orbit control system can be realized by using only a GPS receiver and a cold-gas propulsion system. With a daily-basis atmospheric drag estimation and compensation, the mean orbital radius can be regulated within a few meters around the setpoint.

Although the projection of the mean position error onto the groundtrack displacement was only a few kilometers during the demonstration period, an outer closed-loop control should be introduced to prevent any secular drift in the case of long-term autonomous repeat-groundtrack orbit maintenance.

References

[1] Noreen, G. K., Kerridge, S. J., Ely, T. A., Diehl, R. E., Komarek, T. A., Neelon, J. , and Turner, A., "Daily Repeat-Groundtrack Mars Orbits,"

13th AAS/AIAA Spaceflight Mechanics Meeting, Part 3, 2003, pp. 1143–1157; also American Astronautical Society, Paper 03-179.

[2] Abramson, W. R., Carter, D., Kolitz, S., McConnell, J., Ricard, M., and Sanders, C., "The Design and Implementation of Draper's Earth Phenomena Observing System," *AIAA Space 2001 Conference & Exposition*, AIAA, Reston, VA, 2001.

[3] Bhat, R. S., Frauenholz, R. B., and Cannell, P. E., "TOPEX/Poseidon Orbit Maintenance Maneouver Design," *Advances in the Astronautical Sciences*, Vol. 71, Pt. 1, Aug. 1989, pp. 645–670.

[4] Vincent, M. A., "The Inclusion of Higher Degree and Order Gravity Terms in the Design of a Repeat Ground Track," AIAA/AAS Astrodynamics Conference, Portland, OR, AIAA Paper 90-2899-CP, Aug. 1990.

[5] Ely, T. A., and Howell, K. C., "Long-Term Evolution of Artificial Satellite Orbits Due to Resonant Tesseral Harmonics," *The Journal of the Astronautical Sciences*, Vol. 44, No. 2, 1996, pp. 167–190.

[6] Lara, M., "Repeat Ground Track Orbits of the Earth Tesseral Problem as Bifurcations of the Equatorial Family of Periodic Orbits," *Celestial Mechanics and Dynamical Astronomy*, Vol. 86, No. 2, June 2003, pp. 143–162.

[7] Lamy, A., Chrameau, M.-C.Laurichesse, D., Grondin, M., and Bertrand, R., "Experiment of Autonomous Orbit Control on the Demeter Satellite," *Proceeding of the 18th International Symposium on Space Flight Dynamics*, ESA, Paris, 2004, pp. 327–332.

[8] Fouquet, M., and Sweeting, M. N., "UoSAT-12 Minisatellite for High Performance Earth Observation at Low Cost," *Acta Astronautica*, Vol. 41, No. 3, 1996, pp. 173–182.

[9] Hashida, Y., and Palmer, P. L., "Epicycle Motion of Satellites About an Oblate Planet," *Journal of Guidance, Control, and Dynamics*, Vol. 24, No. 3, May–June 2001, pp. 586–596.

[10] Aorpimai, M., and Palmer, P. L., "Analysis of Frozen Conditions and Optimal Frozen Orbit Acquisition," *Journal of Guidance, Control, and Dynamics*, Vol. 26, No. 5, 2003, pp. 786–793.

[11] Hashida, Y., and Palmer, P. L., "Autonomous Onboard Batch Filter for Near Circular Orbit Determination," *4th ESA International Conference on Spacecraft Guidance, Navigation and Control Systems*, European Space Research and Technology Centre, Noordwijk, South Holland, The Netherlands, 1999, pp. 161–166.

[12] Hashida, Y., and Palmer, P. L., "Analytic Approach for Near-Circular Orbit Determination," AIAA Guidance, Navigation and Control Conference, Montreal, Quebec, Canada, AIAA Paper 2001-4390, Aug. 2001.